Metal Heterostructures | Hot Paper

DOI: 10.1002/ange.201304364

Anisotropic Overgrowth of Metal Heterostructures Induced by a Site-Selective Silica Coating**

*Feng Wang, Si Cheng, Zhihong Bao, and Jianfang Wang**

Anisotropic metal nanostructures exhibit rich morphology-dependent properties.[1–7] First, they possess intriguing plasmonic behaviors and are attractive for various plasmon-based applications.[4,6,7] Second, their surfaces often provide high densities of atomic steps, ledges, and kinks, which can serve as catalytically active sites.[8–10] Third, anisotropic metal heterostructures can exhibit better catalytic properties than monometallic ones, where the presence of one metal can enhance the stability and promote the catalytic performance of the others.[11] Fourth, anisotropic metal nanostructures can function as building blocks for shape-directed formation of unconventional superlattices.[12]

Wet-chemistry approaches are most commonly employed for producing anisotropic metal homo- and heteronanostructures.[2,4,5] Selective molecular capping plays an important role in most anisotropic growth systems.[13–16] For example, during Au nanorod growth, cetyltrimethylammonium bromide (CTAB) molecules are thought to preferentially adsorb on the side facets. The preferential CTAB adsorption slows down the growth on the side facets and promotes the growth at the two ends, leading to the production of Au nanorods.[13,17,18] During the overgrowth of Au/Pd core/shell nanostructures, CTAB molecules adsorb more strongly on the Pd {100} facets, giving cubic and cuboidal structures.[14,19] In other examples, the coating of Au nanorods with polyaniline and adsorption of particular thiol molecules on Au nanospheres induce the production of bimetallic Au/Ag nanostructures with different geometries.[20,21] Selective molecular adsorption can be regarded as a soft templating method. By this means, we have successfully realized transverse overgrowth on Au nanorods.[15] Although the role played by soft templating molecules has been recognized in the growth of anisotropic metal nanostructures, soft templating processes are actually complicated by the delicate interplay among many thermodynamic and kinetic factors, including metal precursor diffusion, interfacial strain, facile equilibrium between adsorbed and free molecules in solutions, facet-dependent metal deposition rates, and molecular bonding strength.[5] As a result, each type of soft template generally functions for a specific material system.

To realize anisotropic overgrowth to obtain metal nanostructures with controlled morphologies, one must stabilize the templating effect. An alternative is to make use of solid materials such as silica as the template. Compared to soft capping molecules, solid materials can be regarded as hard templates. Ideally, hard templates should be deposited on starting metal nanocrystals at desired locations, leaving the uncoated part for further metal deposition. Moreover, hard templates should be robust enough during metal deposition. In this way, hard templating can offer a widely applicable route to anisotropic metal homo- and heterostructures. To date, only one example can be found in this direction, where silica is partially coated on Au nanospheres and serves as a hard template to guide Ag overgrowth on the exposed Au surface.[22]

Herein, we describe a general route to the anisotropic overgrowth of metals on Au nanorods. The overgrowth is enabled by site-selective silica coating. Silica is first selectively deposited at the two ends of the nanorods owing to the higher curvature, or deposited on the side surface when the ends are blocked by thiol-terminated methoxypoly(ethylene glycol) (mPEG-SH). The coated silica layer thereafter guides the overgrowth of metals on the exposed Au surface. The method has been tested for the overgrowth of Au, Ag, Pd, and Pt. In previous experiments, the overgrowth of a second metal on colloidal metal nanocrystals typically ends up with core/shell bimetallic nanostructures.[14,19,23,24] Preferential bonding of soft capping molecules, such as thiolated polymers and molecules, to the ends can induce the overgrowth of Ag and Au on the side surface of Au nanorods, but the deposition of Ag and Au at the ends has been unavoidable.[25,26] In this work, with site-selective silica coating, eight types of unprecedented anisotropic metal nanostructures are produced. Our route therefore is a robust approach for the preparation of metal homo- and heterostructures with designed morphologies and functions.

The starting Au nanorods are stabilized with a CTAB bilayer in aqueous solution (Figure 1a).[27,28] The CTAB bilayer is less ordered and dense at the ends than on the side surface of Au nanorods owing to the larger curvature at the ends.[15,29] Hydrolysis of tetraethyl orthosilicate (TEOS) results in silica coating. In route 1, silica coating dynamics is finely controlled, so that silica is selectively coated at the nanorod ends (Figure 1b), as less energy is needed for removing CTAB molecules at the ends for silica coating. Subsequent overgrowth of a metal takes place at the exposed side surface, leading to transverse metal overgrowth (Figure 1c). In route 2, the ends of the Au nanorods are

[*] Dr. F. Wang,[+] Dr. S. Cheng,[+] Dr. Z. H. Bao, Prof. J. F. Wang
Department of Physics, The Chinese University of Hong Kong
Shatin, Hong Kong SAR (China)
E-mail: jfwang@phy.cuhk.edu.hk

[+] These authors contributed equally to this work.

[**] This work was supported by the Research Grants Council of Hong Kong (CUHK403312, Project Code: 2130320) and National Natural Science Foundation of China (21229101). We thank Mr. Bernd Spliethoff for performing some TEM characterizations.

Supporting information for this article is available on the WWW under http://dx.doi.org/10.1002/anie.201304364.

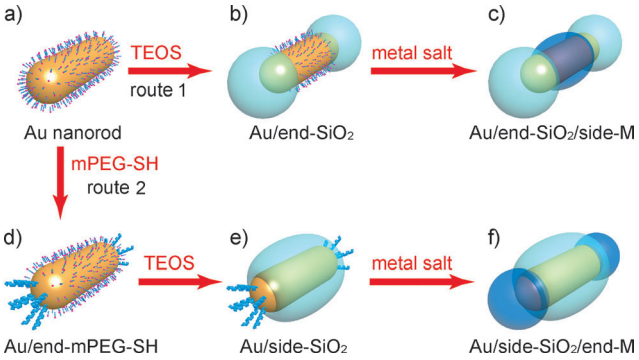

Figure 1. Routes of metal overgrowth. a) Au nanorod capped with a CTAB bilayer. b) Nanorod coated with silica at the ends. c) Nanorod overgrown with a metal on the side surface. d) Au nanorod bonded with mPEG-SH at the ends. e) Nanorod coated with silica on the side surface. f) Nanorod overgrown with a metal at the ends.

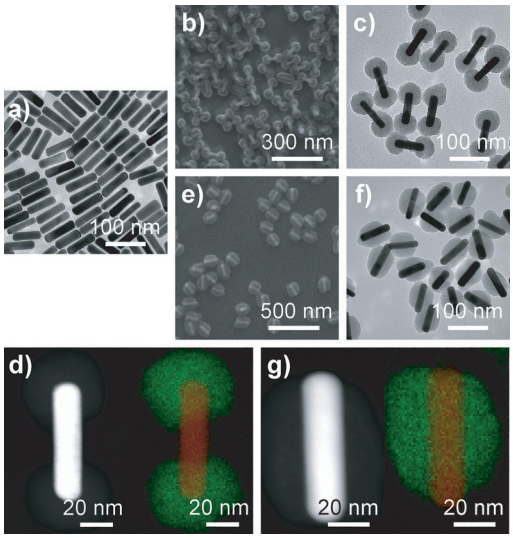

Figure 2. Au nanorods, Au/end-SiO_2, and Au/side-SiO_2 nanostructures. a) Transmission electron microcopy (TEM) image of the starting Au nanorods. b, c) Scanning electron microscopy (SEM) and TEM images of the Au/end-SiO_2 nanostructures. d) Scanning transmission electron microscopy (STEM) image of a single Au/end-SiO_2 nanostructure (left) and its elemental map (right; Au red, Si green). e, f) SEM and TEM images of the Au/side-SiO_2 nanostructures. g) STEM image of a single Au/side-SiO_2 nanostructure (left) and its elemental map (right). The preparations of both samples used 100 μL of the TEOS solution in the first step and 20 μL + 20 μL of the TEOS solution in the second step.

precapped with mPEG-SH (Figure 1 d). The mechanism of the preferential bonding of mPEG-SH to the ends is similar to that for the preferential silica coating at the ends in route 1, where the larger curvature plays an important role. Subsequent silica coating takes place selectively on the side surface under appropriate conditions (Figure 1 e). Because the coated silica is more robust than the adsorbed mPEG-SH molecules in blocking metal overgrowth, the addition of a metal precursor leads to longitudinal overgrowth, where the metal is selectively deposited at the ends of Au nanorods (Figure 1 f).

The average diameter/length of the starting Au nanorods, which were prepared following seed-mediated growth,[13,15,26] are (20 ± 2)/(78±7) nm, respectively (Figure 2 a; see also the Supporting Information, Figure S1). The longitudinal plasmon (LP) peak of the nanorods in aqueous solutions is at 812 nm, and the peak extinction value is 1.93 in a 0.5 cm cuvette. Selective silica coating at the ends was realized through hydrolyzing TEOS at room temperature (for preparation details, see the Supporting Information). The amount of TEOS and reaction time determined the silica layer thickness and overall morphology (Figure S2). In our experiments, the reaction time remained unchanged. Use of small amounts of TEOS resulted in selective silica coating at the nanorod ends. When the TEOS solution volume reached 150 μL, silica was coated both at the ends and on the side surface. Because residual CTAB is existent in the coating solution, silica deposited in this step is mesoporous,[30] and is denoted as $mSiO_2$. The LP peaks of the Au/end-$mSiO_2$ nanostructure solutions, located at ca. 818 nm, are slightly red-shifted compared to that of the starting nanorod sample. Their intensities vary slightly owing to preparation fluctuations. Selective silica coating on the side surface was realized by preferentially bonding mPEG-SH to the ends before TEOS was introduced. mPEG-SH is much larger than CTAB, therefore the preferential bonding of mPEG-SH to the ends caused selective silica coating on the side surface, giving Au/side-$mSiO_2$ nanostructures. The thickness of the coated silica in the Au/side-$mSiO_2$ nanostructures can also be finely controlled by varying the amount of TEOS (Figure S3). With 200 μL of the TEOS solution, the nanorod ends started to be covered with silica. The LP peaks of the Au/side-$mSiO_2$ nanostructure samples were also slightly red-shifted, with small fluctuations in the peak intensity.

The Au@end-$mSiO_2$ and Au@side-$mSiO_2$ nanostructures were subsequently subjected to metal overgrowth by adding them into the growth solution containing the metal source, ascorbic acid as the reducing agent, and cetyltrimethylammonium chloride (CTAC) as the stabilizing agent. The growth of metal nanocrystals in CTAC solutions is much faster than in CTAB ones.[31] Unexpectedly, the overgrowths were not anisotropic or directed by the coated $mSiO_2$ (Figure S4). The growth behaviors also differ among the four metals. For Pd and Au, slight anisotropy in the overgrown nanostructures are observed. On the Au/end-$mSiO_2$ nanostructures, Pd and Au are preferentially deposited on the side surface. On the Au/side-$mSiO_2$ nanostructures, Pd and Au are preferentially deposited at the ends. However, the morphologies are not as clear-cut as designed. For Pt and Ag, relatively uniform deposition of the metals, regardless of the site of the coated $mSiO_2$, is observed. Moreover, careful comparison of the morphologies before and after the metal overgrowths reveals that the coated $mSiO_2$ is reduced in thickness and varied in morphology. The remaining silica layer is visible after Pd and Au overgrowths, but it is nearly completely removed after Pt and Ag overgrowths. The etching of the silica layer is ascribed to the fact that $mSiO_2$ is unstable in neutral and basic solutions.[32] Therefore, metal deposition and silica etching occur simultaneously. The $mSiO_2$ layer is not robust enough to block metal deposition on the coated part of the nanorods. To obtain clear-cut anisotropic metal nanostructures, one must

increase the metal deposition rate and reduce the silica etching rate.

We performed second-step silica coating in a water/ethanol mixture to obtain a more robust silica layer and thus reduce the silica etching rate. Ethanol is a good solvent for CTAB. Silica coating in the mixture produced a solid silica layer, which is denoted as $sSiO_2$. The thickness of the entire silica layer can be finely varied by adjusting the TEOS amount. With small amounts of TEOS, the $sSiO_2$ layer is seen to be preferentially deposited on the pre-coated $mSiO_2$ layer. Electron microscopy characterizations clearly reveal the structure and composition of the resultant Au/end-$mSiO_2$/end-$sSiO_2$ and Au/side-$mSiO_2$/side-$sSiO_2$ (simplified thereafter as Au/end-SiO_2 and Au/side-SiO_2, respectively) nanostructures with small amounts of TEOS (Figure 2b–g). An increase in the amount of TEOS leads to silica coating around the entire nanorod (Figure S5 and S6). The LP peaks of the nanostructures after the second-step silica coating are slightly further red-shifted. Their intensities vary, especially for the Au/side-SiO_2 nanostructures, The peak intensity variation is because these nanostructures can aggregate in water/ethanol mixtures. Aggregation is more severe for the Au/side-SiO_2 nanostructures, because they tend to form linear assemblies, as observed for Au nanorods similarly coated with block copolymers.[33]

Pd overgrowths were first performed to examine the blocking effect of the silica layer coating. Both transverse overgrowth on the Au/end-SiO_2 nanostructures and longitudinal overgrowth on the Au/side-SiO_2 ones were successfully realized (Figure 3a, b, d, e). In transverse overgrowth, Pd nanoparticles are deposited around the circumference at the center of the nanorod. In longitudinal overgrowth, Pd nanoparticles are attached at both ends, increasing the overall length. The deposited Pd nanoparticles are crystalline, as revealed by high-resolution TEM imaging (Figure S7). They are also porous, because Pd tends to form porous structures in CTAC solutions.[31] Elemental mapping clearly shows the composition and geometry of the nanostructures (Figure 3c, f). We also performed Pd overgrowth on the Au nanorods that were end-functionalized with mPEG-SH. Uniform Pd coating is observed, which is similar to what has been obtained in previous studies.[19] This result again points out the importance of using hard templates to realize anisotropic metal overgrowth.

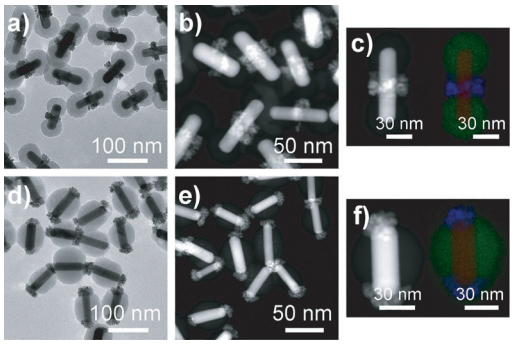

Figure 3. Au/end-SiO_2/side-Pd (top row) and Au/side-SiO_2/end-Pd (bottom row) nanostructures. a) TEM image. b) STEM image. c) STEM image of a single Au/end-SiO_2/side-Pd nanostructure (left) and its elemental map (right; Au red, Pd blue, Si green). d) TEM image. e) STEM image. f) STEM image of a single Au/side-SiO_2/end-Pd nanostructure (left) and its elemental map (right). Both nanostructure samples were prepared with 10 μL of the H_2PdCl_4 solution.

The size of the Pd nanoparticles can be controlled by varying the amount of H_2PdCl_4 (Figure S8). During Pd transverse overgrowth, as the Pd nanoparticles get larger, the LP peak slowly blue-shifts, decreases in intensity, and broadens. The blue-shift, intensity reduction, and broadening arise from plasmon damping owing to the large imaginary part of Pd dielectric function.[14,34] During longitudinal Pd overgrowth, as the Pd nanoparticles become larger, the LP peak red-shifts considerably. At the largest amount of H_2PdCl_4, the peak is located beyond 1200 nm, more than 400 nm longer than the LP wavelength of the starting nanorod sample (Figure S9). The red-shift is also accompanied by peak broadening. The former results from the increase in the overall aspect ratio, whereas the latter comes from the plasmon damping and the non-homogeneous size distribution of the Pd nanoparticles.

Similar to Pd overgrowth, Au overgrowth was also successfully realized in CTAC solutions (Figure 4a, c). Instead of forming porous nanoparticles, the deposited Au atoms

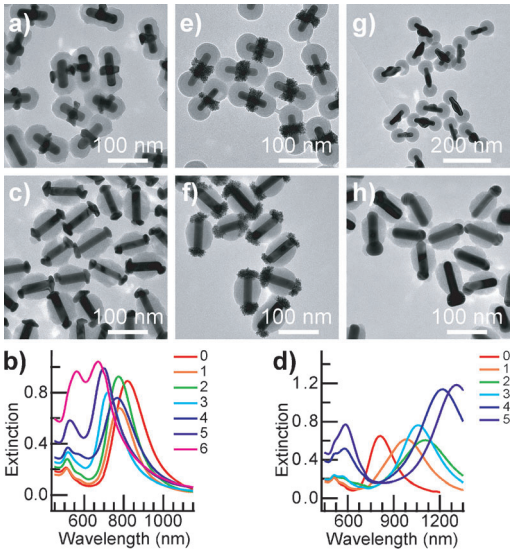

Figure 4. Au/end-SiO_2/side-M (M = Au, Pt, Ag) and Au/side-SiO_2/end-M. a) TEM image of the Au/end-SiO_2/side-Au sample prepared with 10 μL of the $HAuCl_4$ solution. b) Extinction spectra of the Au/end-SiO_2/side-Au samples. Curve 0 is for the Au/end-SiO_2 sample, and curves 1–6 are for the samples prepared with 2 μL, 5 μL, 8 μL, 10 μL, 20 μL, and 40 μL of the $HAuCl_4$ solution, respectively. c) TEM image of the Au/side-SiO_2/end-Au sample prepared with 10 μL of the $HAuCl_4$ solution. d) Extinction spectra of the Au/side-SiO_2/end-Au samples. Curve 0 is for the Au/side-SiO_2 sample, and curves 1–5 are for the samples prepared with 5 μL, 8 μL, 10 μL, 20 μL, and 40 μL of the $HAuCl_4$ solution, respectively. e) TEM image of the Au/end-SiO_2/side-Pt sample prepared with 50 μL of the H_2PtCl_4 solution. f) TEM image of the Au/side-SiO_2/end-Pt sample prepared with 20 μL of the H_2PtCl_4 solution. g) TEM image of the Au/end-SiO_2/side-Ag sample prepared with 10 μL of the $AgNO_3$ solution. h) TEM image of the Au/side-SiO_2/end-Ag sample prepared with 20 μL of the $AgNO_3$ solution.

grow into solid nanoparticles in the uncoated region of the nanorods. The sizes of the Au nanoparticles in both transverse and longitudinal overgrowths can be finely adjusted by changing the amount of $HAuCl_4$ (Figure S10 and S11). The LP peak of the Au/end-SiO_2/side-Au nanostructure samples blue-shifts considerably as the Au nanoparticle at the center of the nanorods increases in size (Figure 4b). In comparison, the LP peak of the Au/side-SiO_2/end-Au nanostructure samples red-shift dramatically as the Au nanoparticles at the ends become larger (Figure 4d). The peak wavelength of the sample prepared with 40 μL of the $HAuCl_4$ solution exceeds 1200 nm. It can be further increased by supplying more Au precursor. Moreover, the LP peak remains strong and relatively narrow after Au overgrowth. This is because the plasmon damping induced by Au overgrowth is much smaller than that induced by Pd overgrowth.

Anisotropic overgrowth is successful for Au and Pd, which grow rapidly in CTAC solutions at room temperature. However, the overgrowth behaviors of Pt and Ag in CTAC solutions are different. Under the same conditions, Pt and Ag overgrowths were not observed, which is attributed to their much smaller growth rates in CTAC solutions at room temperature. When the temperature was increase to 60 °C, small Pt nanoparticles and a continuous Ag layer were found to form in both exposed and silica-coated regions for both transverse and longitudinal overgrowths, even though the coated silica layer was well maintained (Figure S12). The unselective deposition of Pt and Ag is believed to be caused by the enhanced diffusivity of the metal-precursor species into the coated silica layer at the raised temperature. A clear understanding of this phenomenon requires further investigation.

The use of CTAC increases Cl^- concentration in the solution, which in turn stabilizes the metal ions through the formation of complexes. The extent of stabilization varies among different metal ions. To increase the reduction rates for Pt and Ag at room temperature, we examined halogen-free surfactants and found poly(vinylpyrrolidone) (PVP) is a good candidate. PVP can also protect the silica layer and reduce its etching speed.[35] With PVP, both transverse and longitudinal overgrowths of Pt and Ag were successfully realized (Figure 4e–h). Highly porous Pt nanoparticles are formed at the center of the nanorod for transverse overgrowth, and at the ends for longitudinal overgrowth, whereas Ag tends to give solid nanoparticles. As the amount of Pt source is increased, the overgrown Pt nanoparticles become larger, and the LP peak blue-shifts for transverse overgrowth and red-shifts for longitudinal overgrowth. The LP peaks also show plasmon damping (Figure S13), owing to the large imaginary part of Pt dielectric function.[34] The two types of Au/Pt nanostructures were verified by STEM imaging and elemental mapping (Figure S14). Hydroquinone was utilized as the reducing agent for Ag overgrowth, because it can reduce Ag^+ at room temperature. TEM, STEM, and elemental mapping characterizations show that Ag nanoparticles prefer to be deposited on one side or one end of the nanorods, and that this overgrowth behavior is observed more frequently in longitudinal overgrowth (Figure S15 and S16). The asymmetric Ag overgrowth behavior might arise from Ostwald ripening, which drives Ag from one end to the other. Ostwald ripening has been employed to explain the deposition of Au nanoparticles at one end on CdSe nanorods.[36]

In conclusion, selective silica coating on Au nanorods enables us to prepare unprecedented metal nanostructures that are difficult or impossible to produce through soft templating. There are three strengths to our approach: first, the blocking effect of silica, being denser than an adsorbed molecular layer, is stronger; second, highly cross-linked silica cannot flow. In contrast, the free ends of adsorbed molecules can move relatively freely. Third, silica is less prone to dissociate than molecular adsorbates. Even thiol molecules can dissociate, not to mention molecules that adsorb through weak interactions. Molecular dissociation weakens the templating effect, and dissociated molecules can affect metal deposition. On the other hand, our overgrowth results also indicate that, although the location of newly deposited metals is determined by precoated silica, the morphology varies for different metals. Our approach is a promising strategy for designing plasmon-based, application-oriented anisotropic metal nanomaterials.

Received: May 21, 2013
Revised: July 9, 2013
Published online: August 12, 2013

Keywords: anisotropic overgrowth · gold · nanorods · nanostructures · plasmon

[1] R. C. Jin, Y. C. Cao, E. C. Hao, G. S. Métraux, G. C. Schatz, C. A. Mirkin, *Nature* **2003**, *425*, 487.
[2] T. K. Sau, A. L. Rogach, *Adv. Mater.* **2010**, *22*, 1781.
[3] T. K. Sau, A. L. Rogach, F. Jäckel, T. A. Klar, J. Feldmann, *Adv. Mater.* **2010**, *22*, 1805.
[4] H. C. Chen, L. Shao, Q. Li, J. F. Wang, *Chem. Soc. Rev.* **2013**, *42*, 2679.
[5] Y. N. Xia, Y. J. Xiong, B. Lim, S. E. Skrabalak, *Angew. Chem.* **2009**, *121*, 62; *Angew. Chem. Int. Ed.* **2009**, *48*, 60.
[6] N. R. Jana, T. Pal, *Adv. Mater.* **2007**, *19*, 1761.
[7] C. J. Murphy, T. K. Sau, A. M. Gole, C. J. Orendorff, J. X. Gao, L. F. Gou, S. E. Hunyadi, T. Li, *J. Phys. Chem. B* **2005**, *109*, 13857.
[8] B. Lim, M. J. Jiang, P. H. C. Camargo, E. C. Cho, J. Tao, X. M. Lu, Y. M. Zhu, Y. N. Xia, *Science* **2009**, *324*, 1302.
[9] M. A. Mahmoud, C. E. Tabor, M. A. El-Sayed, Y. Ding, Z. L. Wang, *J. Am. Chem. Soc.* **2008**, *130*, 4590.
[10] J. Watt, S. Cheong, M. F. Toney, B. Ingham, J. Cookson, P. T. Bishop, R. D. Tilley, *ACS Nano* **2010**, *4*, 396.
[11] M. S. Chen, D. Kumar, C.-W. Yi, D. W. Goodman, *Science* **2005**, *310*, 291.
[12] M. R. Jones, R. J. Macfarlane, B. Lee, J. Zhang, K. L. Young, A. J. Senesi, C. A. Mirkin, *Nat. Mater.* **2010**, *9*, 913.
[13] M. Z. Liu, P. Guyot-Sionnest, *J. Phys. Chem. B* **2005**, *109*, 22192.
[14] F. Wang, L.-D. Sun, W. Feng, H. J. Chen, M. H. Yeung, J. F. Wang, C.-H. Yan, *Small* **2010**, *6*, 2566.
[15] X. S. Kou, S. Z. Zhang, Z. Yang, C.-K. Tsung, G. D. Stucky, L. D. Sun, J. F. Wang, C. H. Yan, *J. Am. Chem. Soc.* **2007**, *129*, 6402.
[16] B. Lim, H. Kobayashi, T. Yu, J. G. Wang, M. J. Kim, Z.-Y. Li, M. Rycenga, Y. N. Xia, *J. Am. Chem. Soc.* **2010**, *132*, 2506.
[17] B. Nikoobakht, M. A. El-Sayed, *Chem. Mater.* **2003**, *15*, 1957.
[18] T. K. Sau, C. J. Murphy, *Langmuir* **2004**, *20*, 6414.

[19] Y. J. Xiang, X. C. Wu, D. F. Liu, X. Y. Jiang, W. G. Chu, Z. Y. Li, Y. Ma, W. Y. Zhou, S. S. Xie, *Nano Lett.* **2006**, *6*, 2290.
[20] S. X. Xing, Y. H. Feng, Y. Y. Tay, T. Chen, J. Xu, M. Pan, J. T. He, H. H. Hng, Q. Y. Yan, H. Y. Chen, *J. Am. Chem. Soc.* **2010**, *132*, 9537.
[21] Y. H. Feng, J. T. He, H. Wang, Y. Y. Tay, H. Sun, L. F. Zhu, H. Y. Chen, *J. Am. Chem. Soc.* **2012**, *134*, 2004.
[22] T. Chen, G. Chen, S. X. Xing, T. Wu, H. Y. Chen, *Chem. Mater.* **2010**, *22*, 3826.
[23] S. E. Habas, H. Lee, V. Radmilovic, G. A. Somorjai, P. D. Yang, *Nat. Mater.* **2007**, *6*, 692.
[24] F.-R. Fan, D.-Y. Liu, Y.-F. Wu, S. Duan, Z.-X. Xie, Z.-Y. Jiang, Z.-Q. Tian, *J. Am. Chem. Soc.* **2008**, *130*, 6949.
[25] A. Sánchez-Iglesias, E. Carbó-Argibay, A. Glaria, B. Rodríguez-González, J. Pérez-Juste, I. Pastoriza-Santos, L. M. Liz-Marzán, *Chem. Eur. J.* **2010**, *16*, 5558.
[26] W. H. Ni, X. S. Kou, Z. Yang, J. F. Wang, *ACS Nano* **2008**, *2*, 677.
[27] B. Nikoobakht, M. A. El-Sayed, *Langmuir* **2001**, *17*, 6368.
[28] S. Lee, L. J. E. Anderson, C. M. Payne, J. H. Hafner, *Langmuir* **2011**, *27*, 14748.
[29] X. S. Kou, Z. H. Sun, Z. Yang, H. J. Chen, J. F. Wang, *Langmuir* **2009**, *25*, 1692.
[30] I. Gorelikov, N. Matsuura, *Nano Lett.* **2008**, *8*, 369.
[31] F. Wang, C. H. Li, L.-D. Sun, C.-H. Xu, J. F. Wang, J. C. Yu, C.-H. Yan, *Angew. Chem.* **2012**, *124*, 4956; *Angew. Chem. Int. Ed.* **2012**, *51*, 4872.
[32] Y. J. Wong, L. F. Zhu, W. S. Teo, Y. W. Tan, Y. H. Yang, C. Wang, H. Y. Chen, *J. Am. Chem. Soc.* **2011**, *133*, 11422.
[33] T. Chen, H. Wang, G. Chen, Y. Wang, Y. H. Feng, W. S. Teo, T. Wu, H. Y. Chen, *ACS Nano* **2010**, *4*, 3087.
[34] H. J. Chen, F. Wang, K. Li, K. C. Choi, J. F. Wang, Q. Li, L.-D. Sun, X. X. Zhang, H.-Q. Lin, C.-H. Yan, *ACS Nano* **2012**, *6*, 7162.
[35] Q. Zhang, T. R. Zhang, J. P. Ge, Y. D. Yin, *Nano Lett.* **2008**, *8*, 2867.
[36] T. Mokari, C. G. Sztrum, A. Salant, E. Rabani, U. Banin, *Nat. Mater.* **2005**, *4*, 855.